COLLOQUIA: IFA 2010

Volumetric analysis on MRI and PET images for the early diagnosis of Alzheimer's disease

M. Esposito([1]), P. Bosco([1]), L. Rei([1]) and M. Aiello([2])

([1]) *Dipartimento di Fisica, Università di Genova and INFN, Sezione di Genova - Genova, Italy*

([2]) *Dipartimento di Fisica, Università di Napoli and INFN, Sezione di Napoli - Napoli, Italy*

Summary. — In this paper we present the development of a software for the extraction of the hippocampus and surrounding medial-temporal-lobe (MTL) regions from T1-weighted magnetic resonance (MR) and from Positron Emission Tomography (PET) images with no interactive input from the user. With this software we introduce a novel statistical index computed on the intensities in the automatically extracted MTL regions. This index is a measure of gray-matter (GM) atrophy and allows to: distinguish between (a) patients with Alzheimer's disease (AD), patients with amnestic mild cognitive impairment (aMCI), (b) patients with amnestic mild cognitive impairment who will later develop AD in a time frame of 2 years (aMCIconv), and (c) a set of age-matched elderly controls. Once refined, this method could be used to infer about the clinical outcome of aMCI patients.

PACS 87.57.nj – Registration.
PACS 87.57.nm – Segmentation.
PACS 87.57.R- – Computer-aided diagnosis.
PACS 87.61.Tg – Clinical applications.

1. – Introduction

In recent years, the early clinical signs of AD have been extensively investigated, leading to the concept of amnestic mild cognitive impairment (aMCI), an intermediate cognitive state between normal aging and dementia [1-5]. aMCI patients experience memory loss to a greater extent than expected for their age, and they progress to a diagnosis of AD at a faster rate than controls [1,2]. A challenge for modern neuroimaging is to help in the diagnosis of early AD, particularly in aMCI patients.

Three-dimensional (3D) magnetic-resonance imaging with high spatial resolution allows visualization of subtle anatomic changes and thus can help detect brain atrophy in the initial stages of the disease [6]. For this reason, sensitive neuroimaging measures have been investigated to quantify brain structural changes in early AD which are automated
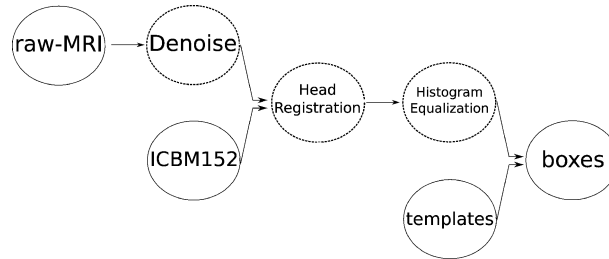
Fig. 1. – The whole workflow process.

enough to permit large-scale studies of the disease and the factors that affect it. To date, these studies have particularly focused on assessing atrophy of medial-temporal-lobe (MTL) structures, including the hippocampus. Hippocampal volumetric measurements typically rely on manual outlining of the MTL structures on serial MR images, which is time consuming and prone to inter-rater and intra-rater variabilities. Thus, large-scale studies of AD-related hippocampal atrophy are often impractical [7]. To accelerate and spread epidemiological studies and clinical trials, some automated systems have been proposed for hippocampal segmentation [8-14], but none is yet widely used due to the high computational burden, unsatisfactory results, or poor generalization capability.

In order to overcome these difficulties, in this work we describe the development of a simple, quick, and operator-independent method to extract two fixed-size ($30 \times 70 \times 30\,\mathrm{mm}^3$), parallelepiped-shaped subimages from a MR image. These subimages contain both the hippocampus and the perihippocampal region; in the following they are denoted as hippocampal boxes (HBs). In order to extend the structural information of the MR images with functional information we also use PET (Positron Emission Tomography) images acquired from the same patients. This approach is based on the hypothesis that structural changes, in this case atrophy, are anticipated by functional changes. So, after an appropriate preprocessing, we extract the two fixed-size HBs from the PET images too.

From the automatically extracted HBs we derive two, intensity-based, statistical indicators, which carefully measure the MTL atrophy and functional changes, and are able to distinguish between patients with AD (with MR and PET index), patients with aMCI, and elderly controls and also between converters and nonconverters to AD within the aMCI population (with MR only) with reasonably good accuracy.

These results are obtained by the analysis of more than 600 MR and 130 PET neuroimages from ADNI database (The Alzheimers Disease Neuroimaging Initiative [15]).

2. – Workflow

From the raw image we extract the hippocampal boxes according to the scheme shown in fig. 1 described in details in this section.

2˙1. *Image preprocessing and registration*. – The used images come from different medical centers and therefore exhibit very different characteristics. These differences concern both the shape and intensity. Therefore, a reasonable and feasible comparison of these heterogeneous images requires an appropriate preprocessing to provide uniform images intensity and a subsequently registration to minimize alignment problems.
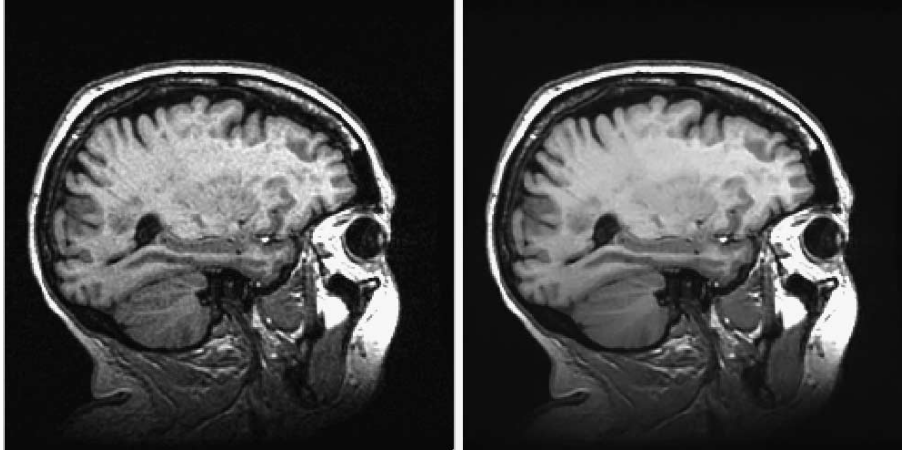
Fig. 2. – An example of noise reduction on an MR image.

2˙1.1. *Noise attenuation.* For MR images an automatic noise reduction has been implemented via steerable pyramids filters [16]. The noise reduction level of the filter is automatically adjusted via threshold calculated with Structural Similarity index. The noise filter has been designed to preserve signal high frequencies and directional components. An example is shown in fig. 2. The PET images, instead, are only preprocessed by a Gaussian filter.

2˙1.2. *Image registration.* All denoised MR images were spatially normalized to stereotactic space (ICBM152) via a multi-step registration. The registration steps consist of a 7-degrees-of-freedom affine transformation, followed by a 12-degrees-of-freedom affine transformation initialized with the transformation parameters of the first step.

This registration process has been realized simultaneously with FLIRT [17] and with *ad hoc* developed modules based on the ITK [18] library. In the first case the metric used has been the cross correlation, in the second the mutual information. The output images of these two different modules have been compared with respect to cross correlation distance from ICBM152 template and the closest has been chosen as the final registration output (fig. 3). The preprocessed PET images, instead, were spatially normalized to stereotactic space (ICBM152) via a 7-degrees-of-freedom affine transformation.
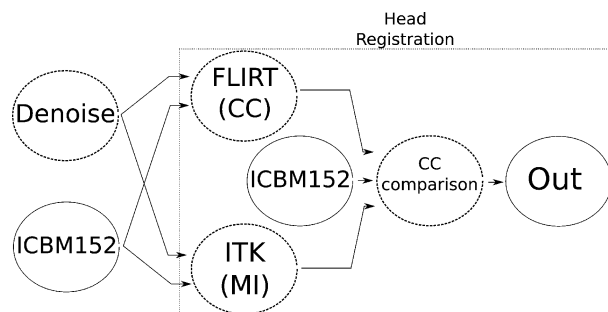

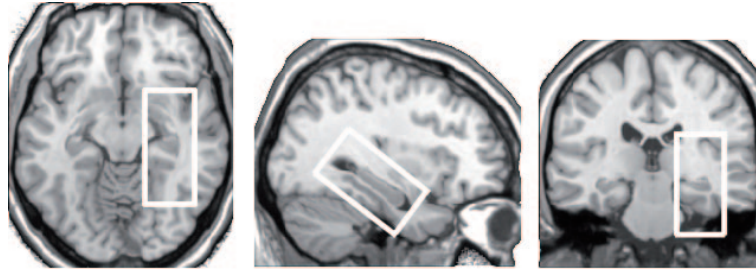Fig. 3. – The MR registration workflow.

Fig. 4. – Axial, sagittal and coronal views of an image after alignment with the ICBM152 template. On the three slices an outline of the right hippocampal box is also shown.

The registration normalizes the brains in terms of dimensions, position, and spatial orientation. Consequently, all hippocampi share similar positions and orientations. Three slices cut from a 3D MR image after spatial normalization and the outline of the hippocampal ROI are shown in fig. 4.

All images were resampled to make them isotropic with voxel size of $(1 \times 1 \times 1\,\mathrm{mm}^3)$.

$2\dot{}2$. *Histogram normalization*. – In order to obtain images with homogeneous intensity, an intensity histogram normalization is carried out. In practice, we consider the intensity histogram of a subimage of ICBM152 template. We choose this subimage so that it contains gray matter, white matter and CSF only; a small volume around the ventricular region proves to fulfill this request and it turns out to be very easy to register. The same intensity histogram is calculated on the target image to be normalized. Then we define a mapping from the centroids (corresponding to gray matter, white matter and CSF) of the target image to the template ones. The calculated function is applied to the complete image. Figure 5 shows the differences between the intensity histograms of all dataset before and after normalization.

$2\dot{}3$. *MRI templates extraction*. – The extraction method relies on the fact that the gray level contrast displayed by the hippocampal formation and adjacent structures is unique all over the brain. Therefore, a procedure can be developed to identify the hippocampal region unambiguously. Neuroanatomical considerations suggested the size of a HB as a $(30 \times 70 \times 30\,\mathrm{mm}^3)$ parallelepiped-shaped box (sizes of right-to-left, posterior-to-anterior,
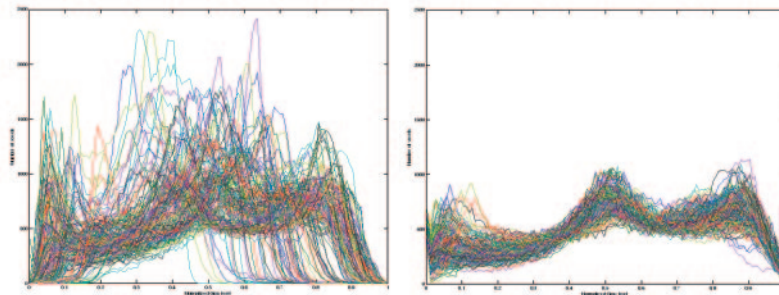

Fig. 5. – Effect of the normalization on the intensity histograms.

and inferior-to-superior directions, respectively). The extraction of the HBs (right and left) was performed with an automatic procedure, that required minimal interactive intervention.

2˙3.1. *Extraction of the hippocampal boxes.* All the N MR scans were labeled and denoted as $MR_{(i)} = 1, \ldots, N$. The first HB was manually extracted by an expert reader from $MR_{(1)}$, the scan of a healthy control displaying minimal atrophy. Particular care was applied in the positioning of the box boundaries in order to place the hippocampal formation in the inner portion of the box. The next step of the procedure consists in extracting the second HB from the remaining $N - 1$ MR images. The extraction procedure is based on the registration of the first HB (the *fixed image*) onto the remaining $N - 1$ images (the *moving images*) via a 6-degrees-of-freedom rigid transformation (three translational and three rotational degrees of freedom). The success of the registration of each moving image onto the fixed image is quantified by the minimum reached in distance values where the distance provides a measure of how well the transformed moving image matches the fixed image. In this way a quantitative criterion is assigned for finding the optimal values of the transformation parameters. We adopted a definition of distance based on the normalized correlation coefficient C. This distance is scale and shift invariant and it produces a cost function with sharp peaks and well-defined minima. Thus, for each $N - 1$ images this operation produces a value of distance and the six geometrical parameters, three translations and three rotation angles. From the image with minimum distance value the second box is extracted, this box takes the role of fixed image and its registration parameters are used to initialize the registration of remaining $N - 2$ images for the following step. The procedure for the progressive extraction of all HBs follows this scheme and stops once the whole sample of N images has been processed and N HBs have been obtained.

2˙3.2. *Templates selection.* When a new hippocampal box is needed we could apply the method showed in **2**˙3.1 on $N + 1$ images. This would be obviously very time consuming and with the increasing of images number totally unfeasible. We show that the extraction can be successfully performed by a smaller number of properly chosen HBs, in the following denoted as HB templates (HBTs). The basic idea of the HBT selection process is to create groups of HBs, or clusters, in such a way that the HBs in the same cluster are near and the HBs belonging to different clusters are far. Here we denote by $d_{i,j}$ $(i, j = 1, \ldots, N)$ the distance (normalized correlation coefficient) between $HB_{(i)}$ and $HB_{(j)}$. Thus, each HB can be considered as a point belonging to an N-dimensional space $N = 63000$ ($30 \times 70 \times 30$) and whose distances from all other HBs are known. The classication of the N HBs in homogeneous clusters is performed following this procedure:

1. starting from N clusters we obtain $N - 1$ clusters simply grouping the first closest two;

2. calculate again $d_{i,j}$ $(i, j = 1, \ldots, N - 1)$ where, instead of the boxes grouped at the previous step, we consider their cluster centroid;

3. iterate until we obtain only two clusters.

To illustrate the clustering we use a dendrogram as shown in fig. 6. The problem is rapresented by the choice of the *natural* number of clusters rapresenting the hippocampalboxes population. This problem has been solved analyzing the centroids distance distribution *vs.* the number of clusters. As expected the resulting natural number of clusters
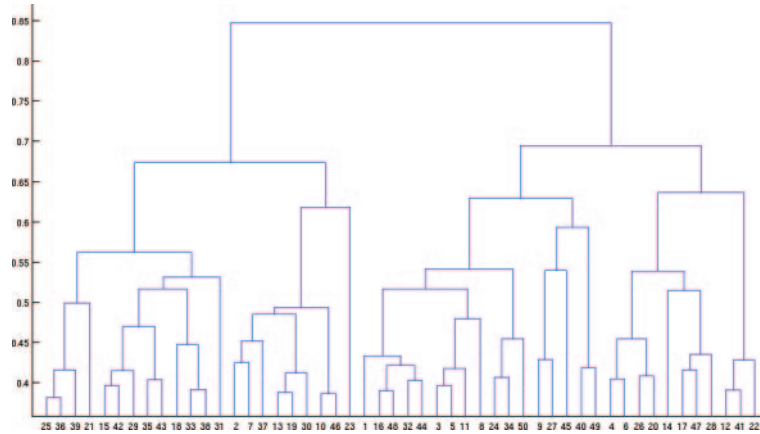
Fig. 6. – Dendrogram. On the x-axis the cluster index, on the y-axis the cluster distance.

is independent of the amount of boxes considered (if statistically consistent) and for the hippocampal boxes it is about 10. The centroids of the found clusters are the searched HBT.

2˙3.3. *Extraction of the hippocampal boxes from* new image. Each new image (*i.e.* not included in the N used for the templates selection) was rigid registered onto the n HBTs of sect. **2**˙3.2, obtaining, in this way, n possibile candidates. The one with the best registration metric value among these was chosen as the searched hippocampal box. This procedure is done independently for both left and right hippocampal box with relative HBTs.

2˙3.4. Extraction of the hippocampal boxes from PET image. For the hippocampal boxes extraction from PET images we simply follow these steps:

1. registration, with mutual information, via a 7-degrees-of-freedom affine transformation of the preprocessed (sect. **2**˙1.1) PET on the respective MR image;

2. boxes extraction from the PET from the same position determined for the extraction of the boxes from the MR image.

3. – Volumetric analysis

In this section we describe the process that, from MR and PET hippocampal boxes, lead to two statistical indicators, which measure MTL atrophy and functional loss. In order to emphasize the discriminant features between normal, AD and aMCI we apply different filters on the HBs. These filters are both intensity and structural based, namely: Gaussian, average, entropy, range, and standard deviation, all applied with different kernel dimensions ($3{\times}3{\times}3$, $5{\times}5{\times}5$ and $7{\times}7{\times}7\,\mathrm{mm}^3$). The features space is represented by $30 \times 70 \times 30\times$ (number of filters), then, in order to reduce the dimensionality of the classification problem, we apply a machine learning technique called Random Forest [19]. The reduced features space (fig. 7) is fed into different classifiers (both Random Forest and SVM [20] are used) and we obtain the two indexes, one for the MRI and one for the PET.
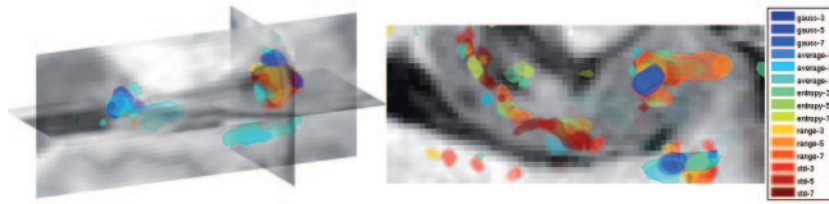
Fig. 7. – Example of relevant features selected by Random Forest for different filters.

4. – Result

Significant differences of MTL atrophy index (for MR images), measured by the SVM and RF method, were detected both in AD and in aMCI cohorts. In figs. 8 and 9 we can see the box plot of the atrophy index for normal, aMCI, aMCIconv and AD groups obtained by SVM and Random Forest, respectively. With both classifiers there is an evident separation from normal and AD indexes with an area under the receiver operating characteristic (ROC) curve, which indicates the relationship between sensitivity and 1-specificity for each intergroup discrimination, of 0.98 for SVM and 0.95 for Random Forest classifier. As expected the aMCI group index takes intermediate values between normal and AD groups indexes. The aMCIconv group index values are nearer to the AD index than to the aMCI index.

Looking at PET images, we find again significant differences among AD and in aMCI cohorts compared to normal cohort. In fig. 10, we can see the box plot of the functionality index for normal, aMCI and AD groups obtained by SVM classifier. In this case too, there is an evident separation from normal and AD indexes with an area under the ROC curve of 0.86. The aMCI group index takes intermediate values between normal and AD groups indexes.
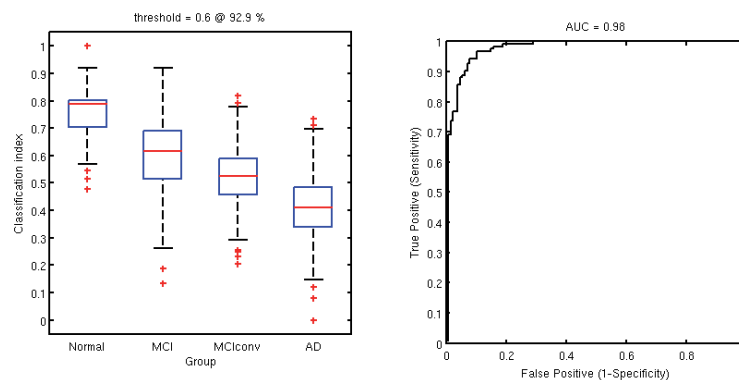

Fig. 8. – (Colour online) Box plot of normal, aMCI, aMCIconv and AD group atrophy MRI indexes according to SVM classifier. Red lines represent the median, boxes the interquartile range, and whiskers the range; stars = outliers. The area under the ROC curve is 98%.
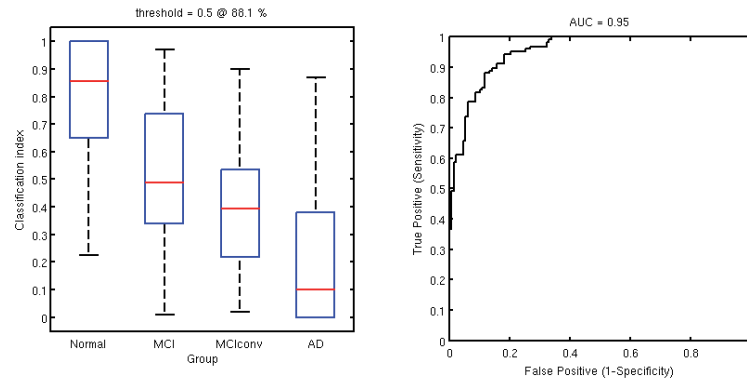
Fig. 9. – Box plot of normal, aMCI, aMCIconv and AD group atrophy MRI indexes according to Random Forest classifier. The area under the ROC curve is 95%.

5. – Conclusion

In this work we showed a method that, from a brain MR image, automatically extracts a small volume around both hippocampi (the hippocampal boxes) and provides statistical indicators able to separate the AD, aMCI, aMCIconv and controls cohorts. Moreover, with a PET image of the same patient, we were able to extract the corresponding boxes and obtain another statistical indicator, based on functionality instead of anatomical changes, that can also discriminate AD from normal cohorts. Since it is well known that MTL atrophy is associated with declining cognitive function [21], we showed that our method is able to capture differences between subgroups of interest with different stages of cognitive impairment, with comparable discriminating capability between aMCI converters and controls, and between AD patients and controls. This result should be considered with caution owing to the relatively small number of converters. Anyway, this is in agreement with several studies regarding manual segmentation of hippocampus, which have reported that the baseline hippocampal volume is an indicator of future progression to AD [21-25]. This is also in agreement with studies based on visual
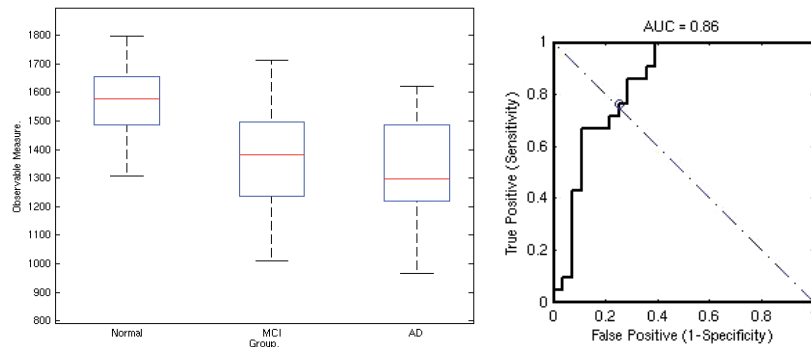

Fig. 10. – Box plot of normal, aMCI and AD group functionality PET indexes according to SVM classifier. The area under the ROC curve is 86%.

rating, which clearly found MTL atrophy in patients who subsequently converted to AD [26-28]. Compared to other methods of hippocampal or MTL atrophy measurement, our method does not directly tackle the objective of hippocampus segmentation. The procedure is fully automated and allows the analysis of large sets of data and requires relatively moderate image postprocessing and pre-requisites for automation. Therefore, it could be a good candidate for being more widely used than other automatic methods. PET results, even though preliminary and not comparable with those obtained with MR boxes analysis, are very interesting and promising because they underline the significance of the hippocampal region in functional images, in contrast to other previous studies [29, 30]. Moreover, according to the hypothesis that functional changes could anticipate anatomical changes, the PET hippocampal-region analysis could be an earlier indicator of the progress of Alzheimer's disease. In conclusion, we report an original procedure for assessing MTL atrophy based on intensity measurement in a standardized perihippocampal volume using established T1-weighted volumetric scans and for assessing MTL functionality based on intensity measurement in PET scan. These measures significantly differentiates patients with AD from controls and MCI converters from controls with MR analysis, and patients with AD from controls with PET analysis. The technique is simple to use and may be of value in clinical practice for an early diagnosis of AD, without the need for expert assessment or labor intensive manual measures.

REFERENCES

[1] Petersen R. C., Smith G. E., Waring S. C., Ivnik R. J., Tangalos E. G. and Kokmen E., *Arch. Neurol.*, **56** (1999) 303, PMID: 10190820, URL http://www.ncbi.nlm.nih.gov/pubmed/10190820.

[2] Petersen R. C., Doody R., Kurz A., Mohs R. C., Morris J. C., Rabins P. V., Ritchie K., Rossor M., Thal L. and Winblad B., *Arch. Neurol.*, **58** (2001) 1985, PMID: 11735772, URL http://www.ncbi.nlm.nih.gov/pubmed/11735772.

[3] Dubois B. and Albert M. L., *Lancet Neurol.*, **3** (2004) 246, PMID: 15039037, URL http://www.ncbi.nlm.nih.gov/pubmed/15039037.

[4] Petersen R. C., *J. Int. Med.*, **256** (2004) 183, PMID: 15324362, URL http://www.ncbi.nlm.nih.gov/pubmed/15324362.

[5] Winblad B., Palmer K., Kivipelto M., Jelic V., Fratiglioni L., Wahlund L., Nordberg A., Bäckman L., Albert M., Almkvist O., Arai H., Basun H., Blennow K., de Leon M., DeCarli C., Erkinjuntti T., Giacobini E., Graff C., Hardy J., Jack C., Jorm A., Ritchie K., van Duijn C., Visser P. and Petersen R. C., *J. Int. Med.*, **256** (2004) 240, PMID: 15324367, URL http://www.ncbi.nlm.nih.gov/pubmed/15324367.

[6] Kantarci K. and Jack C. R., *NeuroRx: J. Am. Soc. Exp. NeuroTher.*, **1** (2004) 196, PMID: 15717020, URL http://www.ncbi.nlm.nih.gov/pubmed/15717020.

[7] Carmichael O. T., Aizenstein H. A., Davis S. W., Becker J. T., Thompson P. M., Meltzer C. C. and Liu Y., *NeuroImage*, **27** (2005) 979, PMID: 15990339, URL http://www.ncbi.nlm.nih.gov/pubmed/15990339.

[8] Barnes J., Scahill R. I., Boyes R. G., Frost C., Lewis E. B., Rossor C. L., Rossor M. N. and Fox N. C., *NeuroImage*, **23** (2004) 574, PMID: 15488407, URL http://www.ncbi.nlm.nih.gov/pubmed/15488407.

[9] Crum W. R., Scahill R. I. and Fox N. C., *NeuroImage*, **13** (2001) 847, PMID: 11304081, URL http://www.ncbi.nlm.nih.gov/pubmed/11304081.

[10] Fischl B., Salat D. H., Busa E., Albert M., Dieterich M., Haselgrove C., van der Kouwe A., Killiany R., Kennedy D., Klaveness S., Montillo A., Makris N., Rosen B. and Dale A. M., *Neuron*, **33** (2002) 341, PMID: 11832223, URL http://www.ncbi.nlm.nih.gov/pubmed/11832223.

[11] HOGAN R. E., MARK K. E., WANG L., JOSHI S., MILLER M. I. and BUCHOLZ R. D., *Radiology*, **216** (2000) 291, PMID: 10887264, URL http://www.ncbi.nlm.nih.gov/pubmed/10887264.

[12] POWELL S., MAGNOTTA V. A., JOHNSON H., JAMMALAMADAKA V. K., PIERSON R. and ANDREASEN N. C., *NeuroImage*, **39** (2008) 238, PMID: 17904870, URL http://www.ncbi.nlm.nih.gov/pubmed/17904870.

[13] WANG L., BEG F., RATNANATHER T., CERITOGLU C., YOUNES L., MORRIS J. C., CSERNANSKY J. G. and MILLER M. I., *IEEE Trans. Med. Imaging*, **26** (2007) 462, PMID: 17427733, URL http://www.ncbi.nlm.nih.gov/pubmed/17427733.

[14] YUSHKEVICH P. A., PIVEN J., HAZLETT H. C., SMITH R. G., HO S., GEE J. C. and GERIG G., *NeuroImage*, **31** (2006) 1116, PMID: 16545965, URL http://www.ncbi.nlm.nih.gov/pubmed/16545965.

[15] *Alzheimer's disease neuoroimaging initiative (ADNI)*, http://www.loni.ucla.edu/ADNI/ (2007), URL http://www.loni.ucla.edu/ADNI/.

[16] SIMONCELLI E. P. and FREEMAN W. T., *The steerable pyramid: A flexible architecture for multi-scale derivative computation*, in *Proceedings of the International Conference on Image Processing, 23-26 Oct. 1995, Washington, DC, USA*, *Proc. IEEE*, **3** (1995) 444.

[17] FISCHER B. and MODERSITZKI J., *Flirt: A flexible image registration toolbox*, in *Proceedings of Biomedical Image Registration: Second International Workshop, WBIR 2003* (Springer-Verlag) 2003, pp. 261–270.

[18] YOO T., ACKERMAN M., LORENSEN W., SCHROEDER W., CHALANA V., AYLWARD S., METAXES D. and WHITAKER R., *Engineering and algorithm design for an image processing API: a technical report on ITK. The insight toolkit*, in *Proceedings of Medicine Meets Virtual Reality*, edited by WESTWOOD J. (IOS Press, Amsterdam) 2002, pp. 586–592.

[19] BREIMAN L., *Mach. Learn.*, **45** (2001) 5.

[20] CORTES C. and VAPNIK V., *Mach. Learn.*, **20** (1995) 273.

[21] JACK C. R., PETERSEN R. C., XU Y. C., O'BRIEN P. C., SMITH G. E., IVNIK R. J., BOEVE B. F., WARING S. C., TANGALOS E. G. and KOKMEN E., *Neurology*, **52** (1999) 1397, PMID: 10227624, URL http://www.ncbi.nlm.nih.gov/pubmed/10227624.

[22] TAPIOLA T., PENNANEN C., TAPIOLA M., TERVO S., KIVIPELTO M., HÄNNINEN T., PIHLAJAMÄKI M., LAAKSO M. P., HALLIKAINEN M., HÄMÄLÄINEN A., VANHANEN M., HELKALA E., VANNINEN R., NISSINEN A., ROSSI R., FRISONI G. B. and SOININEN H., *Neurobiol. Aging*, **29** (2008) 31, PMID: 17097769, URL http://www.ncbi.nlm.nih.gov/pubmed/17097769.

[23] DEVANAND D. P., PRADHABAN G., LIU X., KHANDJI A., SANTI S. D., SEGAL S., RUSINEK H., PELTON G. H., HONIG L. S., MAYEUX R., STERN Y., TABERT M. H. and DE LEON M. J., *Neurology*, **68** (2007) 828, PMID: 17353470, URL http://www.ncbi.nlm.nih.gov/pubmed/17353470.

[24] CONVIT A., DE ASIS J., DE LEON M. J., TARSHISH C. Y., SANTI S. D. and RUSINEK H., *Neurobiol. Aging*, **21** (2000) 19, PMID: 10794844, URL http://www.ncbi.nlm.nih.gov/pubmed/10794844.

[25] JACK C. R., SHIUNG M. M., WEIGAND S. D., O'BRIEN P. C., GUNTER J. L., BOEVE B. F., KNOPMAN D. S., SMITH G. E., IVNIK R. J., TANGALOS E. G. and PETERSEN R. C., *Neurology*, **65** (2005) 1227, PMID: 16247049, URL http://www.ncbi.nlm.nih.gov/pubmed/16247049.

[26] DECARLI C., FRISONI G. B., CLARK C. M., HARVEY D., GRUNDMAN M., PETERSEN R. C., THAL L. J., JIN S., JACK C. R. and SCHELTENS P., *Arch. Neurol.*, **64** (2007) 108, PMID: 17210817, URL http://www.ncbi.nlm.nih.gov/pubmed/17210817.

[27] GEROLDI C., ROSSI R., CALVAGNA C., TESTA C., BRESCIANI L., BINETTI G., ZANETTI O. and FRISONI G. B., *J. Neurol. Neurosurg. Psychiatry*, **77** (2006) 1219, PMID: 16891386, URL http://www.ncbi.nlm.nih.gov/pubmed/16891386.

[28] DE LEON M. J., GOLOMB J., GEORGE A. E., CONVIT A., TARSHISH C. Y., MCRAE T., SANTI S. D., SMITH G., FERRIS S. H. and NOZ M., *Am. J. Neuroradiol.*, **14** (1993) 897, PMID: 8352162, URL http://www.ncbi.nlm.nih.gov/pubmed/8352162.

[29] Ishii K., Soma T., Kono A. K., Sofue K., Miyamoto N., Yoshikawa T., Mori E. and Murase K., *J. Nucl. Med.*, **48** (2007) 704.
[30] Mevel K., Desgranges B., Baron J., Landeau B., Sayette V., Viader F., Eustache F. and Chételat G., *Neuroimage*, **37** (2007) 18.